ACS OMEGA

Open Access

http://pubs.acs.org/journal/acsodf

Article

Study on the Influence of Supercritical CO_2 with High Temperature and Pressure on Pore-Throat Structure and Minerals of Shale

Xiangzeng Wang, Xiao Sun,* Xing Guo, Liming Zheng,* and Pan Luo

Cite This: *ACS Omega* 2024, 9, 15259−15270

Read Online

ACCESS | Metrics & More | Article Recommendations

ABSTRACT: Injection of carbon dioxide offers substantial social and economic advantages for reduction of carbon emission reduction. Utilizing CO_2 in shale formations can significantly enhance the extraction of shale oil or gas. Conducting fundamental research on how CO_2 affects shale rock's physical properties is crucial for enhancing its porosity and permeability. Particularly for deep shale layers, the effects of supercritical CO_2 on shale physical properties should be investigated at a high temperature and pressure, differing from the standard conditions applied in shallower layers. A study examined the impact of supercritical CO_2 under such conditions on the pore-throat structure and mineral composition of the shale. The experimental parameters included immersing shale rock in supercritical CO_2 at pressures ranging from 10 to 70 MPa and temperatures between 55 and 95 °C. This study evaluated changes in mineral composition, pore-throat structure (using scanning electron microscopy and nitrogen adsorption tests), and the porosity and permeability of the shale rocks. Findings indicated that the dissolution of CO_2 altered the relative content of certain minerals. The average quartz content rose and, potassium feldspar and the average contents of plagioclase declined conversely. When increasing the pressure, an increase in the relative content of I/S mixed layer and a decrease in illite content were observed and kaolinite content experienced minor changes. When increasing the temperature, kaolinite, I/S mixed layer, and chlorite all exhibited a decreasing trend with increasing temperature, while the relative contents of illite increased. Some of the pores become rounded in a high-magnification view under the impact of CO_2 dissolution. Additionally, the Brunauer−Emmett−Teller specific surface area, pore volume, porosity, and permeability generally improved with increasing pressure and temperature. With the temperature and pressure of CO_2 increased, the curves of nitrogen absorption had moved first upward and then downward. However, under specific CO_2 conditions, the permeability enhancement effect could diminish or even negatively impact the shale's permeability. These findings underscore the need to optimize supercritical CO_2 injection parameters under high-temperature and high-pressure conditions. This research aims to provide theoretical guidance for the efficient use of CO_2 in deep shale applications to increase the shale gas output.

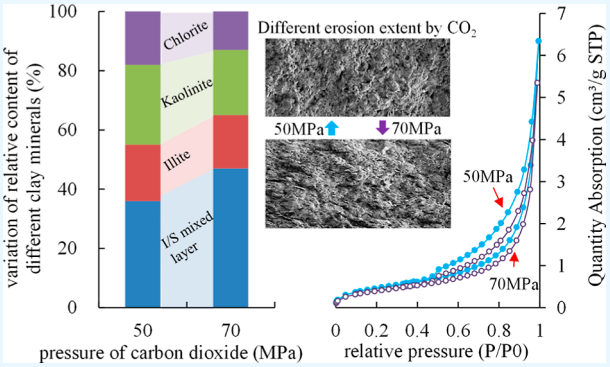

1. INTRODUCTION

Carbon dioxide utilization boasts significant social and economic benefits for reducing carbon emissions via geological storage and oil reservoir stimulation. CO_2 injection has emerged as an important method for enhancing oil recovery. Experimental tests and simulations have been undertaken to evaluate the improvement of recovery by CO_2 injections.[1−3] In the context of the shale oil and gas field, CO_2 can be used to stimulate the development of shale oil and gas via adsorption and replacement processes. Researchers have carried out experimental and dynamic simulation studies on CO_2-enhanced recovery in shale formations.[4,5] These experimental analysis included mechanical characterization, modification in pore-throat structures, alterations in mineral content, changes in adsorption−desorption, and variations in pore and permeability levels.[6−8] Existing experimental studies conducted under conventional temperature and pressure settings have found that the interaction between CO_2 and reservoir rocks considerably influences the rock properties. The interaction of rock−CO_2−water often results in the dissolution of the rock matrix and its cementing substance. This interaction process simultaneously involves the transport of debris particles and the deposition of asphaltenes in the porous media.[9,10] The combined effect led to changes in the pore structure and permeability of the reservoir rock. However, it might be a disputable result. For example, Tian et al. (2023) found that

Received: December 7, 2023
Revised: March 9, 2024
Accepted: March 14, 2024
Published: March 25, 2024

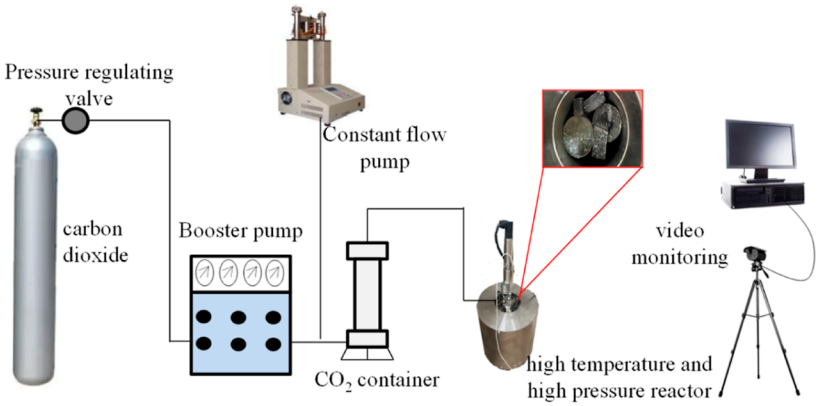

Figure 1. Experimental equipment for shale rock exposure to high-temperature and high-pressure carbon dioxide.

Table 1. XRD Analysis before CO_2 Reaction

mineral compositions (%)	quartz	potassium feldspar	plagioclase	calcite	pyrite	I/S mixed layer	Illite	kaolinite	chlorite
values	37.9	12.4	16.8	3.1	2.1	9.7	8.3	5.3	4.4

porosity and permeability increased with time, and in their experiments, CO_2 exposure with dry or wet shale core in a reactor lasted for days.[11] The ultralow permeability of shale might contribute to a permeability reduction, as reported in conventional core flooding tests in Jafari Behbahani et al. (2015).[12] Previous experimental work by Shen and Sheng (2017) also demonstrated severe permeability damage caused by the asphaltene deposition during CO_2 huff-n-puff injection in Eagle Ford shale core plugs.[13] The variations in porosity and permeability in shale formations are influenced by a multitude of factors, including asphaltene deposition, mineral erosion, transportation of minerals, and deposition of particles. These factors play critical roles in altering the physical structure and characteristics of shale reservoirs, impacting the efficiency of resource extraction and the overall integrity of the geological formation. The state of carbon dioxide, particularly its temperature and pressure, also has a significant impact on the pore-throat structure and minerals of the shale. These varying states can affect how CO_2 interacts with shale, influencing its ability to penetrate pore spaces, interact with minerals. These findings underline the complex and multifaceted nature of using CO_2 injections in both conventional and unconventional reservoir settings. This information supports the development of more efficient and effective strategies for carbon dioxide utilization in oil and gas recovery.

Current research on CO_2 replacement, fracturing, and rock characterization in shale is performed under specific pressure and temperature conditions. Particularly for deep shale reservoirs (deeper than 3500 m) or operations involving high pressure, such as during hydraulic fracturing,[14−16] there is a pressing need for more experimental testing and theoretical analysis on high temperature and pressure. These studies are essential to understand the mechanisms of microscopic changes in rock structure under extreme conditions of high temperature and pressure. Additionally, it is important to examine the interaction between various states of CO_2 and reservoir rocks, their impact on the rocks' physical properties, and to develop appropriate experimental and theoretical simulation methods. Certainly, Xie et al. (2021) made an investigation on the adsorption characteristics of CH_4 and CO_2 in shale at high pressure (0−25 MPa) and temperature (30−100 °C).[17] Xie et al. (2023) studied the pressure (3−8 MPa), temperature (20−80 °C) and pore structure sensitivity in the CO_2/methane competitive adsorption system in shale gas reservoirs.[18] Currently, the conditions set for CO_2 exposure or CO_2 driving primarily reflect conventional temperature and pressure environments, typically below 60 °C in temperature and 20 MPa in pressure.[8,19,20] Research simulating the effects of CO_2 injection on rock properties under these extreme conditions is still limited. For applications involving CO_2 in deeper formations or under significant pressure, it is crucial to consider elevated temperature and pressure levels.

In this study, the impact of CO_2 exposure on the physical properties of shale rock, such as the porosity, mineral composition, and microstructure, is quantitatively evaluated under high-temperature and high-pressure conditions. The pressure settings ranged from 10 to 70 MPa, and temperatures varied between 55 and 95 °C. This research is aimed at providing theoretical guidance for the geological storage of CO_2 in deep reservoirs and advancing the development of shale oil and gas fields.

2. MATERIALS AND METHODS

2.1. Experimental Materials and Equipment. The experimental apparatus included a high-temperature and high-pressure reactor (Figure 1), drying oven, balance, video monitoring equipment, vacuum saturation device, vernier calipers, porosity meter, permeability meter, X-ray diffractometer, ASAP 2460 surface area and porosity analyzer, scanning electron microscope, and so on.

The experimental materials included: shale rock from Chang 7 layer in Ordos basin (porosity about 0.89%, permeability about 0.06×10^{-3} μm^2), distilled water, $CaCl_2$, carbon dioxide gas, seals. The samples used in experimental groups were identical to nearby positions in one core. The experimental shale was mainly composed of quartz, potassium feldspar, plagioclase, calcite, pyrite, siderite, and clay minerals (Table 1). Quartz was the most abundant mineral, accounting for about 37.9%, while clay minerals accounted for about 27.7%. The clay minerals in shale were dominated by an illite−smectite mixed layer (I/S mixed layer, 35%), followed by Illite (30%), with a small amount of kaolinite and chlorite.

https://doi.org/10.1021/acsomega.3c09698
ACS Omega 2024, 9, 15259−15270

2.2. Experimental Method. First, pretreatment of shale cores was done. The columnar cores were cleaned, dried, and weighed. The cores were vacuumed and then saturated with simulated water ($CaCl_2$ type, 20,000 mg/L salinity) for over 12 h.

Second, CO_2 exposure process was followed. The shale rock was soaked in contact with supercritical carbon dioxide. Then, the core was placed in the reactor, connecting temperature and pressure sensors and the CO_2 gas injection line. CO_2 was initially injected at a low pressure of 5 MPa, followed by a sealing test to check for gas leaks. The temperature and gas pressure were gradually increased to the predetermined levels. For pressure sensitivity, the range was set between 10 and 70 MPa at a constant temperature of 45 °C (Table 2). For temperature sensitivity, the range was 55−95 °C at a constant pressure of 25 MPa. The core is exposed to CO_2 for a period of 24 h. Post-exposure, the reactor is disassembled and the cores were removed, dried, and weighed.

Table 2. Shale Sample Treatment with CO_2

sample	temperature (°C)	pressure (MPa)
contrast group (no CO_2 treatment)		
Y-0		
Y-1	55	25
Y-2	70	25
Y-3	95	25
Y-4	45	10
Y-5	45	30
Y-6	45	50
Y-7	45	70

Third, physical property testing was done. The physical property tests were carried out on the shale cores. The tests were performed in a specific order to avoid damaging the cores' appearance and internal structure.

X-ray diffraction (XRD) mineral composition and pore-throat analysis with nitrogen adsorption, porosity, and permeability were measured. The measurement was compared to evaluate the influence of CO_2 conditions on the physical properties of the shale rock under high temperature and pressure. Data were recorded and compared for analysis.

Then porosity and permeability measurements were conducted. The porosity of shale rock after the CO_2 reaction was measured with a porosity meter. Helium gas was used to inject into the shale rock. The porosity value was obtained by measuring the apparent rock volume and particle volume. The permeability of shale rock after the CO_2 reaction was obtained by an air injection test.

Scanning electron microscopy (SEM) was conducted. SEM can provide high-resolution images that allow the observation of nanoscale structures. The surface topology of the shale samples was characterized by high-resolution SEM. SEM experiments were conducted using an H-800 SEM. The

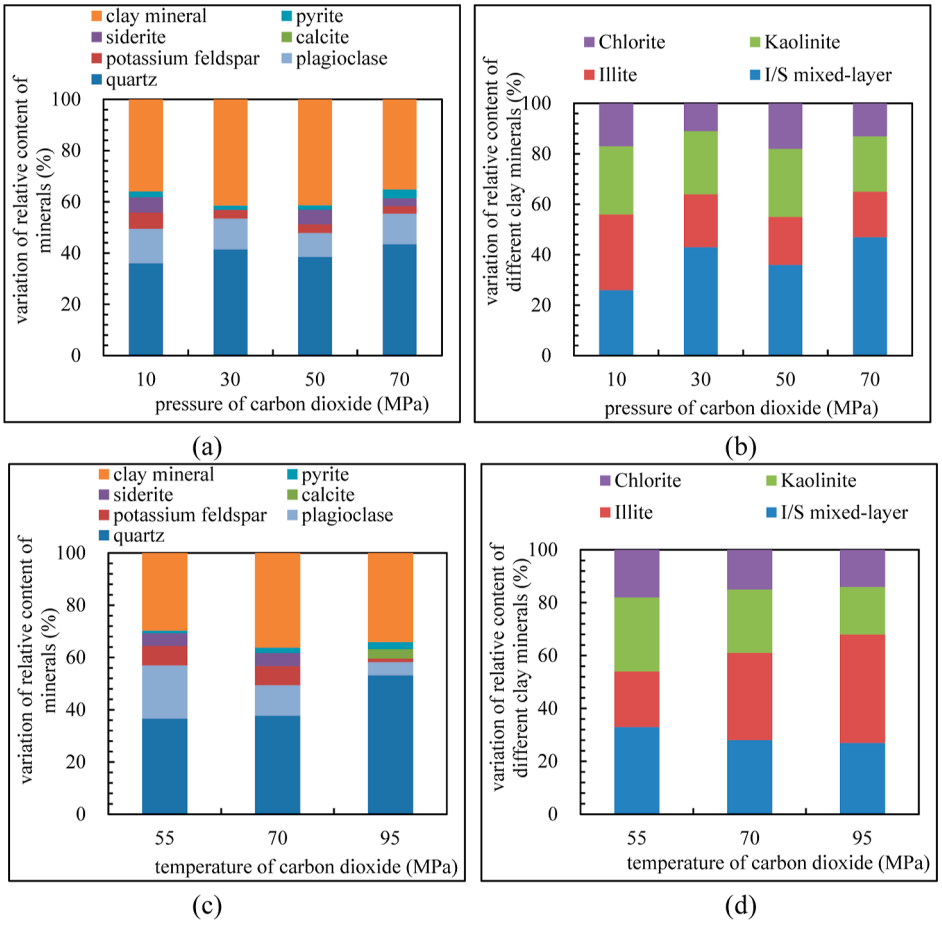

Figure 2. Influence of pressure and temperature of carbon dioxide on the relative content of minerals in shale rock (a) relative content of minerals under different pressure; (b) relative content of clay minerals under different pressure; (c) relative content of minerals under different temperature; (d) relative content of clay minerals under different temperature.

https://doi.org/10.1021/acsomega.3c09698
ACS Omega 2024, 9, 15259−15270

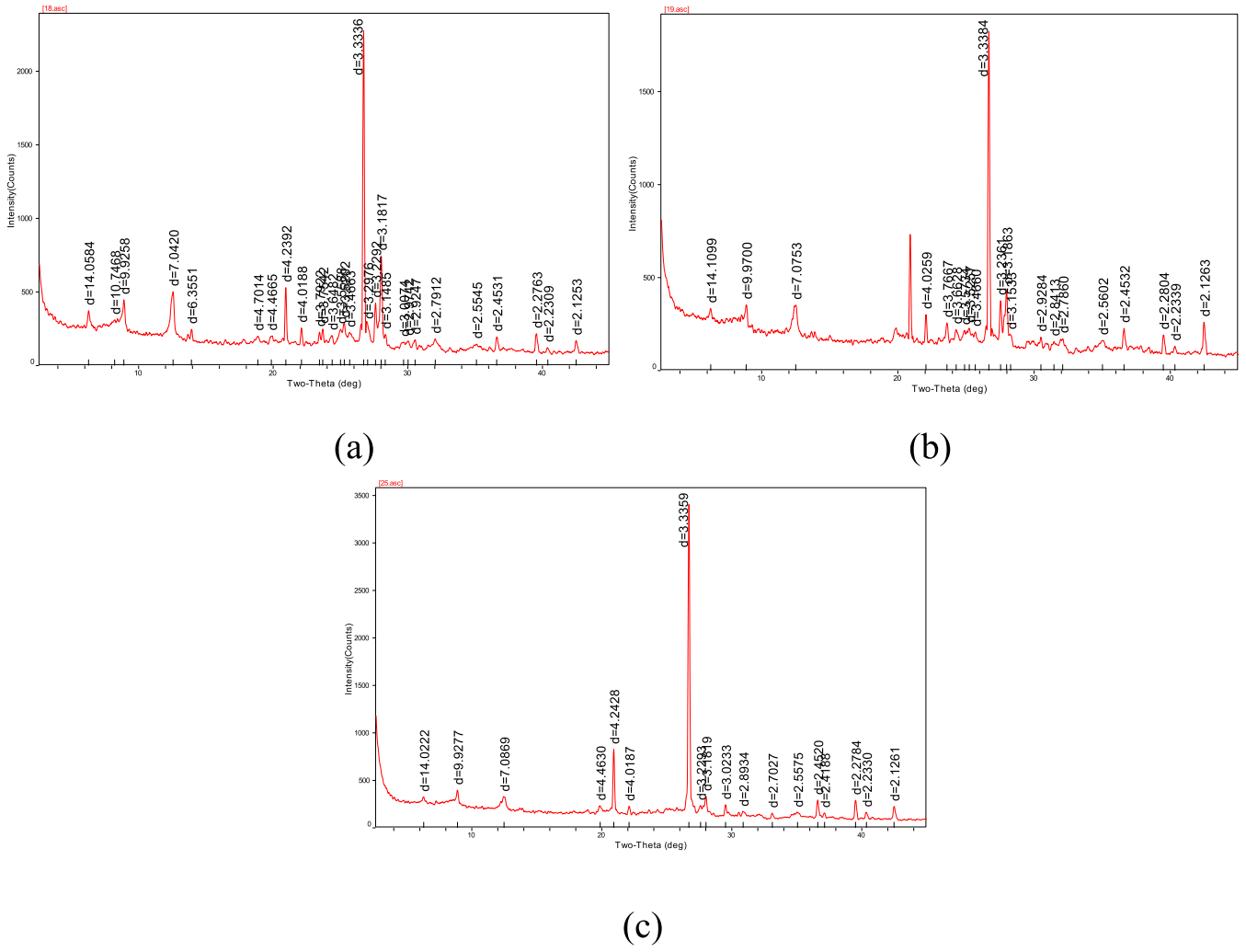

Figure 3. XRD results of shale rock with CO_2 treatment under different temperature (a) 55 °C and 25 MPa, sample Y-1; (b) 75 °C and 25 MPa, sample Y-3; (c) 95 °C and 25 MPa sample Y-3.

samples were cut, and part of samples (diameter less than 1 cm) was used for treatment. Multiple sites were selected for imaging and feature relocation. The images with 100 and 10 μm (magnification) were shown in the results. The result also reveals the relative abundance of elemental data used to infer minerals are present.

Nitrogen adsorption test was then conducted. The low pressure nitrogen adsorption method was chose to characterize the shale's pore structure. The nitrogen adsorption−desorption isotherms were obtained at a temperature of 196 °C with a relative pressure (P/P_0) range of 0.0025−0.99 using a Micrometritics ASAP 2460 system. The average pore diameter (desorption), Brunauer−Emmett−Teller (BET)-specific surface area, and total pore volume (D < 40.3122 nm) could be obtained from the nitrogen adsorption−desorption data.

Finally an X-ray diffraction mineral composition analysis was done. Part of the samples were cut and ground into powder. X-ray diffractometer (XRD) measurements were performed by using a TTRIII type X-ray diffractometer. Separate testing of clay and nonclay minerals was done with powder less than 10 μm and that less than 2 μm.

3. RESULTS

3.1. Influence on the Minerals of Shale Rock. As recent studies had indicated that the action of CO_2 in shale rock was correlated with mineral content, the study was to explore the effect of CO_2 on the mineral composition of shale from the Chang 7 layer in the Ordos basin. During operations such as CO_2 injection or CO_2 fracturing, the CO_2 was under high-temperature and high-pressure conditions. This study uniquely focused on the mineral transformations and variations in content under specific CO_2 conditions, contrasting with those of traditional states. The variation of mineral content influenced by CO_2 was shown in Figure 2.

Under high temperature (55−95 °C), the average quartz content rose to 42.5%, surpassing the initial value. Conversely, potassium feldspar, and plagioclase witnessed a decline, averaging 5.3 and 12.4%, respectively, both falling below their initial concentrations.

Under high pressure (30−70 MPa), consistent with the thermal conditions, quartz content again exceeded the initial value, averaging 41.1%. A further reduction was observed in potassium feldspar, down to 3.2%, and plagioclase, to 11.1%, both also lower than their starting points.

The mineral content of shale showed significant variations when subjected to increasing pressure in the presence of

https://doi.org/10.1021/acsomega.3c09698
ACS Omega 2024, 9, 15259−15270

supercritical CO_2. This fluctuation can be attributed primarily to two factors: the inherent inhomogeneity of the shale and the chemical reactions occurring within shale minerals due to the CO_2 exposure. There was a general decrease in the relative content of plagioclase and potassium feldspar. The relative content of clay minerals exhibited considerable fluctuation, influenced by several processes including the dissolution-conversion of clay minerals, the formation of precipitates, the generation of feldspar dissolution debris, and particle transport dynamics. A slight increase in the relative contents of quartz and pyrite was noted, with changes in iron-bearing minerals serving as vital indicators of clay mineral dissolution. Calcite was prone to dissolution and observed less frequently. An increase in the relative content of I/S mixed layer and a decrease in illite content were observed. Chlorite content fluctuated in a manner consistent with the overall trend of clay minerals. Kaolinite content experienced minor changes. The dominant clay mineral shifted from I/S mixed layer to illite with increasing temperature, while at elevated pressures, I/S mixed layer remained predominant. Figure 3 presents the change in the XRD spectra of the CO_2-treated samples under different temperature. Changes in mineral content among different samples were evident. Particularly notable were the variations observed around 22−28° in the two-theta (deg) range of Figure 3. These changes suggest that a variety of minerals were affected by high-pressure supercritical carbon dioxide, altering the physical properties of the rock.

The relative contents of plagioclase and potassium feldspar exhibited a decreasing trend with rising temperature during CO_2 injection above 55 °C. Conversely, the relative contents of clay minerals and quartz increased. Kaolinite, I/S mixed layer, and chlorite all exhibited a decreasing trend with increasing temperature, while the relative contents of illite increased.

3.2. Influence on the Microscale Pore Throat of Shale Rock. The microscale pore throat of shale rock was assessed through scanning electron microscope (SEM) and nitrogen adsorption tests.[21,22] The SEM results were utilized for a qualitative analysis of the shale rock dissolution. Meanwhile, nitrogen adsorption results were employed for a quantitative assessment of punctate variation.[23−25]

3.2.1. The Change of Microscale Pore Throat by Scanning Electron Microscope. The SEM test in Figure 4 revealed poorly developed pores in shale, dominated by illite (and I/S mixed layer), feldspar, pyrite, and other minerals. Various types of pore throats were identified in the experimental shale including intergranular pores, intercrystal pores, secondary dissolution pores, organic matter pores, and cracks. Intergranular pores were found between primary mineral grains, encompassing compacted pore spaces resulting from clastic sediments during diagenesis, as well as micropore spaces between clay minerals, primarily illite and chlorite. Nanoscale pores were abundant within organic matter, while slit- or wedge-shaped pores developed between shale lamellae or along feldspar structural surfaces, sometimes filled with cement. Cracks were identified as the main channels for fluid seepage in shale, effectively enhancing the oil and gas permeability.

When CO_2 enters the supercritical state, it had the effect of mineral dissolution with its high diffusivity, ultralow viscosity, and surface tension. During the experiments, it was observed that the rock surface was dissolute with distinct dissolution pores. Some of the pores become rounded in high-

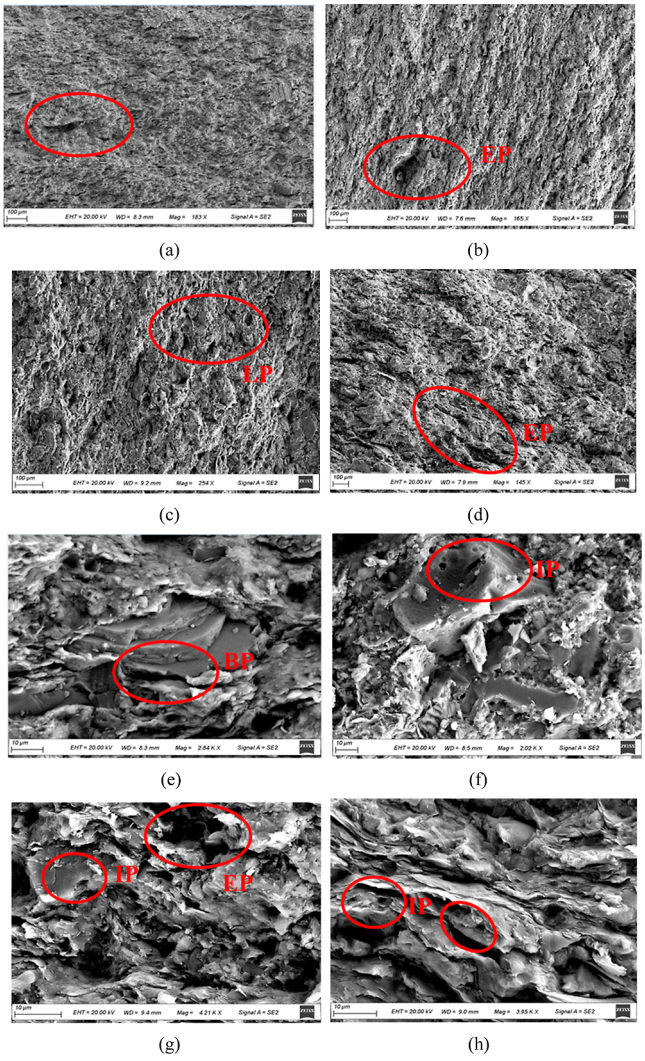

Figure 4. Influence of pressure and temperature of carbon dioxide on the microscale pore throat by SEM test (a,e) untreated; (b) 30; (c) 50; (d) 70 MPa; (f) 55; (g) 75; (h) 95 °C.

magnification view. Except for the minor pores in Figure 4a,e, the large pore in Figure 4a was with an irregular outer bound. In Figure 4b,g, the out bound of intergranular pores showed a trend toward sphericity. There existed many intercrystal dissolved pores in Figure 4f,g (noted IP) which were with a spherical out round. With enhanced exposure to carbon dioxide, the number of pores increased. In Figure 4a, there were only a small number of large pores with a magnification view of 100 μm. In Figure 4c,d, the amount of large pores increased obviously; and part of the cracks could be seen in Figure 4d. The pores were mainly intergranular, as shown in Figure 4e. There were intragranular dissolved pores and intergranular pores in Figure 4f,g. Some of the intragranular dissolved pores extended to cracks with a small width, as shown in Figure 4h. The dissolution effect of potassium feldspar and plagioclase was evident. Additionally, a small number of quartz deposits were observed, aligning with the findings in Section 3.1.

3.2.2. The Change of Microscale Pore Throat by Nitrogen Adsorption. The nitrogen adsorption tests on the shale showed that the hysteresis rings are of the IUPAC classification H3 type (Figure 5). Based on the results of the nitrogen

https://doi.org/10.1021/acsomega.3c09698
ACS Omega 2024, 9, 15259−15270

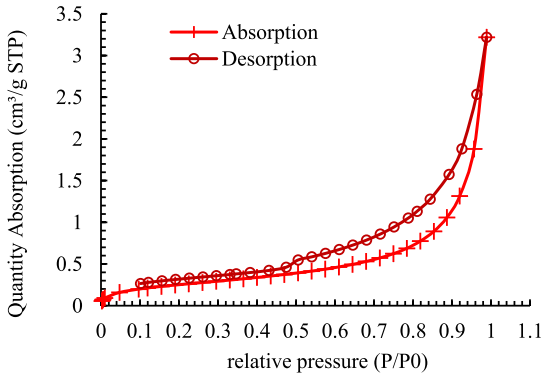

Figure 5. Absorption and desorption curve before CO_2 treatment.

adsorption test on the samples, the nitrogen adsorption curve generally presented four stages.[29,30] In the extremely low pressure stage ($P/P_0 < 0.05$), the micropores are sequentially filled, and the initial isotherm of the sample containing micropores showed a significant large and steep increase. In the low-pressure stage ($0.05 < P/P_0 < 0.45$), the overall curve rose slowly, only showing a weak knee-like bend in the initial stage. This stage showed monolayer adsorption, where nitrogen molecules formed a thin layer on the entire adsorbent surface. In the medium pressure stage ($0.45 < P/P_0 < 0.80$), the adsorption curve entered the plateau region, and the adsorption amount increased linearly with relative pressure. During this stage, nitrogen molecules had undergone surface multilayer adsorption. The high-pressure stage ($0.80 < P/P_0 < 1.00$) was the capillary condensation zone for nitrogen adsorption, and the adsorption capacity rapidly increased with relative pressure.

It indicated that the pore structure was not homogeneous, and slotted pores appeared to be composed of flaky particles. The result reflected the presence of parallel plate-like slit-type pores in the sample. The rock was mainly of micropores, with an average pore diameter (absorption) of 10.52 nm. When analyzed with the desorption data and BJH method, the pore size distribution seems to be mainly single peak type, and a fake peak occurred of pore radius near 3.8 nm. The pore radius character was analyzed again with the absorption curve (Figure 6). Considering the location of the pore peak of the samples, the shale from nitrogen adsorption experiment had more fine mesopores of 4−10 nm and some coarse mesopores of 10−50 nm. In this pore characteristic, shale oil is prone to adsorption and aggregation but is not conducive to fluid seepage. At the same time, the BJH theoretical equation and BET equation was used to obtain total pore volume and BET-specific surface area.[31] The BET-specific surface area was 0.9538 m^2/g and the total pore volume ($D < 40.3122$ nm) was 0.002556 cm^3/g.

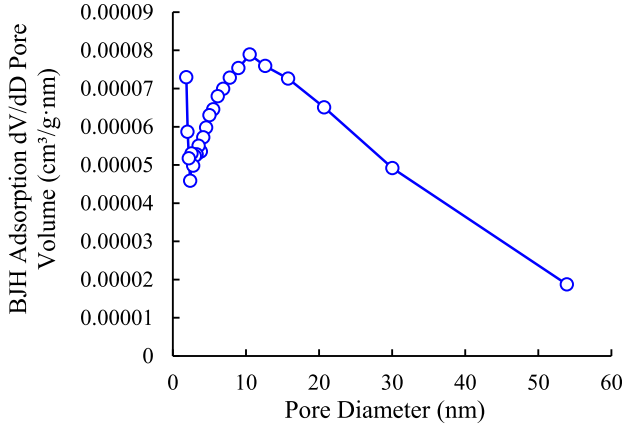

Figure 6. Distribution of pore structure before CO_2 treatment from nitrogen adsorption test.

The hysteresis rings of shale rocks with CO_2 treatment are of the IUPAC H3 type. Figure 7 shows the absorption curve and desorption curve when the rocks were treated under different CO_2 temperature. Though with similar curve shapes, the curves had move along the vertical axis direction. With the temperature and pressure of CO_2 increased, the curves had moved first upward and then downward. With the temperature and pressure increased, the package area has relatively first increased and then decreased. Certainly, the increase of package area was relatively small.

When the nitrogen adsorption tests were carried out on rocks which are immersed in carbon dioxide at different pressures (in Figure 8), the average BET-specific surface ranged between 1.480 and 1.733 m^2/g and, the average total pore volume ($D < 40.3122$ nm) was between 0.0051 and 0.0060 cm^3/g. When the nitrogen adsorption tests were carried out on rocks which are immersed in carbon dioxide at different temperatures, the average BET-specific surface ranged between 1.621 and 1.964 m^2/g, and the average total pore volume ($D < 40.3122$ nm) ranged from 0.0056 to 0.0066 cm^3/g.

The average BET-specific surface and average total pore volume first increased and then decreased with an increasing pressure and temperature of CO_2. The effect of temperature on specific surface and pore volume was greater than that of pressure. The tests indicated that the number of microspores appeared to increase, and the space increased under the influence of CO_2. However, there was also a situation that the volumes of some pores decreased and the permeability declined, due to particle transport, crystallization and precipitation inner these pores under high temperature and pressure.

3.3. The Change of Porosity and Permeability. The temperature of the CO_2 had a significant effect on the porosity and permeability of the shale as in Figures 9 and 10. The values of porosity and permeability of the shale samples prior to the reaction by CO_2 were also presented in the figures, and the samples were the same. Compared to the control group, both the porosity and permeability of shale were generally increased by CO_2. With the increase of the action temperature, the permeability shows a trend of first increasing and then decreasing, with a range of increase from 0.1 to 1.2 mD; both the gas test porosity and the porosity determined by nitrogen adsorption testing showed an overall increasing trend, with a range of increase from 0.07 to 1.25%. The result indicated that under high temperature action the dissolution reaction of CO_2 with shale minerals was stronger, increasing the pore space. However, the accompanying particle transport and secondary mineral growth during dissolution process could also weaken the trend of permeability improvement.[20,26]

The effect of the CO_2 pressure on the porosity and permeability of shale was also evident (Figure 10). Shale porosity tended to increase monotonically with increasing CO_2 action pressure, with an increase range of 0.41−0.84%. However, permeability showed different variations at different pressures (10−50 MPa), with an overall increase range of 0.4−0.6 mD. The decrease in permeability at the experimental pressure of 70 MPa might be partly due to the non-

https://doi.org/10.1021/acsomega.3c09698
ACS Omega 2024, 9, 15259−15270

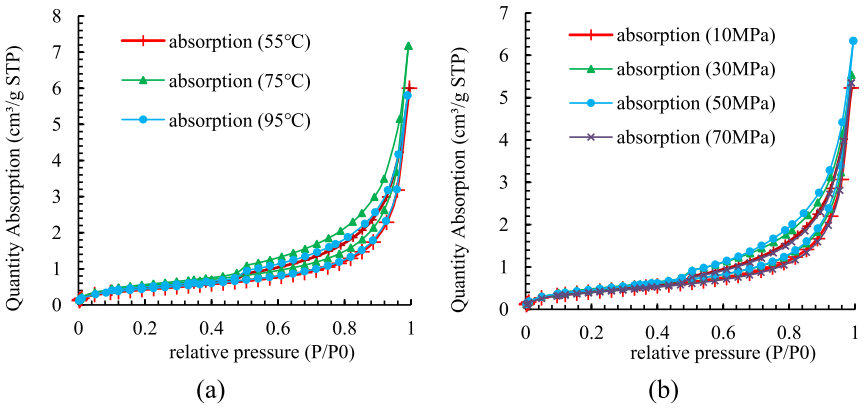

Figure 7. Absorption curve and desorption curve under different CO_2 temperature and pressure (a) variation under different temperature; (b) variation under different pressure.

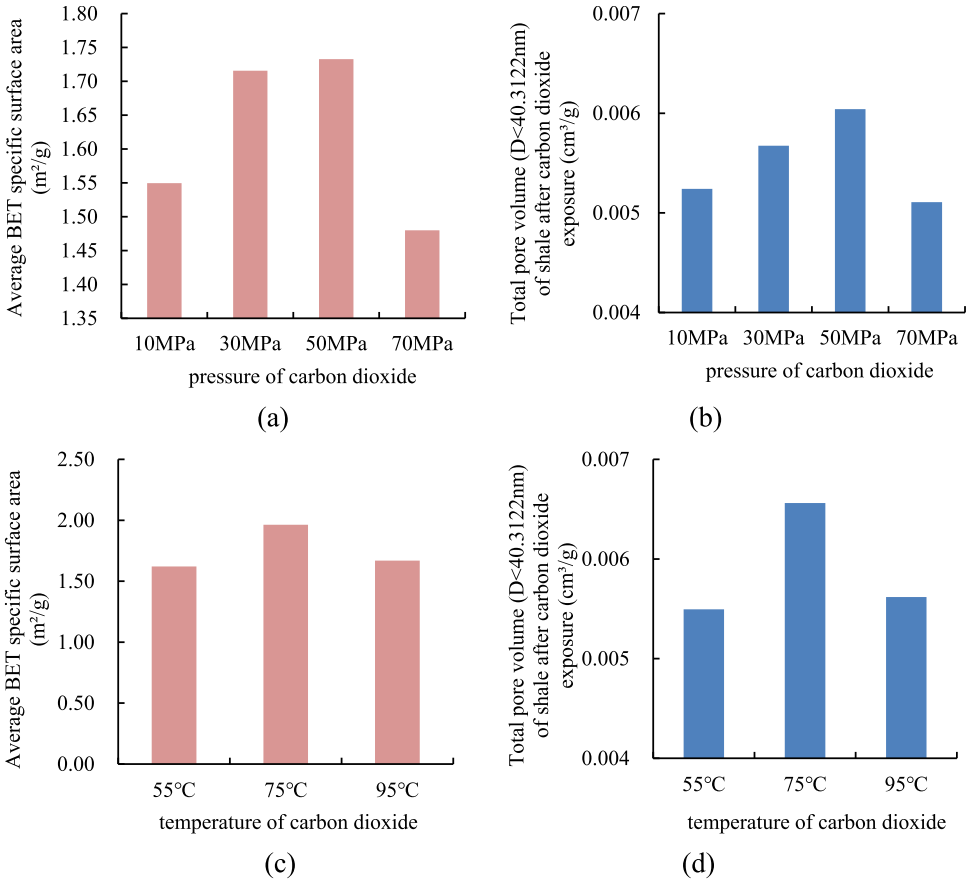

Figure 8. Average BET-specific surface area and total pore volume (D < 40.3122 nm) of shale after carbon dioxide treatment (a) surface area under different pressure; (b) pore volume under different pressure; (c) surface area under different temperature; (d) pore volume under different pressure.

homogeneity of the core and partly due to the particle transport and secondary mineral growth, which caused permeability damage. In contrast to pressure conditions, temperature had a stronger influence on the variation of porosity and permeability through the CO_2 reaction.

4. DISCUSSIONS

4.1. Mineral Reaction under the Impact of CO_2. This suggests that the feldspar and clay minerals in the shale, when exposed to supercritical CO_2 under high-temperature and high-pressure conditions, underwent significant chemical dissolution, accompanied by a slight growth of secondary microquartz.[27−29] Additionally, in an acidic environment, calcium ions existed in an ionic state and reacted with carbon dioxide to form calcium bicarbonate. Upon pressure release, bicarbonate ions and clay minerals were easily transported by the expanding seeping action of carbon dioxide. White precipitates of calcium bicarbonate were observed on the shale rock surface (disappearing upon prolonged heating or dampening).

Based on the experimental results, the series of chemical reactions between shale minerals and supercritical carbon

https://doi.org/10.1021/acsomega.3c09698
ACS Omega 2024, 9, 15259−15270

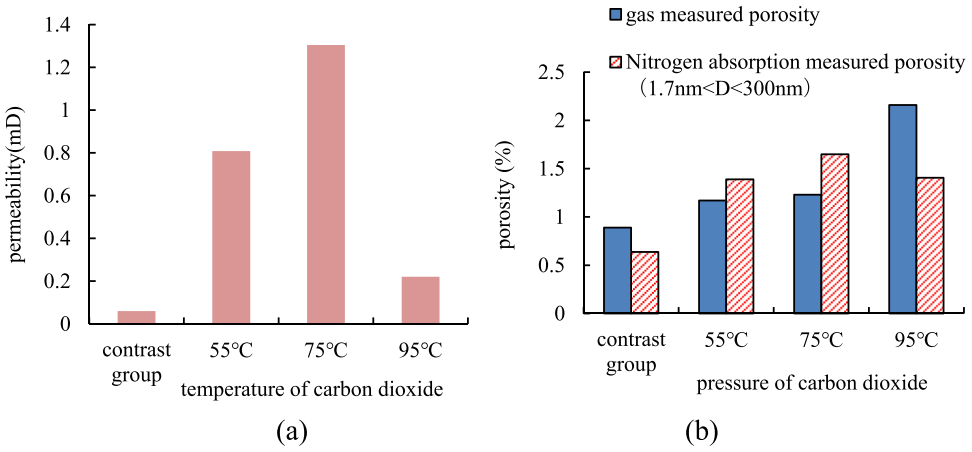

Figure 9. Porosity and permeability of shale after carbon dioxide treatment under different high temperature (a) permeability; (b) porosity.

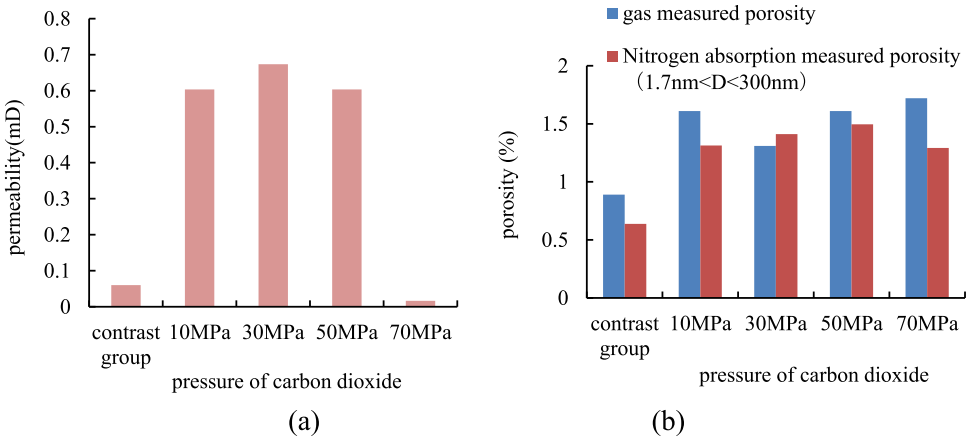

Figure 10. Porosity and permeability of shale after carbon dioxide treatment under different high pressures (a) permeability; (b) porosity.

dioxide (which is acidic when dissolved in water) under high temperature and pressure is outlined below. The equation for feldspar reactions is given in eq 1; the equation for calcite reaction is provided in eq 2; the equation for illite reaction is expressed in eq 3; and the equation for chlorite reaction is detailed in eq 4.[30−32]

$$\mathrm{NaAlSi_3O_8 + 4H_2O + 4H^+ \rightarrow Na^+ + Al^{3+} + 3H_4SiO_4}$$

$$\mathrm{CaAl_2Si_2O_8 + H^+ + HCO_3^- + H_2O \rightarrow CaCO_3 + Al_2Si_2O_5(OH)_4}$$

$$\mathrm{2KAlSi_3O_8 + 9H_2O + 2H^+ \rightarrow 2K^+ + 4H_4SiO_4 + Al_2Si_2O_5(OH)_4} \quad (1)$$

$$\mathrm{CaCO_3 + H^+ + HCO_3^- \rightarrow Ca^{2+} + 2HCO_3^-} \quad (2)$$

$$\mathrm{Illite + 8H^+ \leftrightarrow 0.6K^+ + 2.3Al^{3+} + 0.25Mg^{2+} + 3.5SiO_2 + 5H_2O} \quad (3)$$

$$\mathrm{Mg_3Fe_2Al_2Si_3O_{10}(OH)_8 + 16H^+ \leftrightarrow 2Al^{3+} + 3Mg^{2+} + 2Fe^{2+} + 3SiO_2 + 12H_2O} \quad (4)$$

With the reaction, the experimental results improved the improvement of microscale pore throat of shale rock through SEM and nitrogen adsorption.

The observed phenomenon of bound variation of microscale pores was attributed to two main factors. First, the low value of the sodium/potassium ion ratio in the simulated water resulted in the selective dissolution of plagioclase feldspar. Second, the injection of acidic fluids promoted the dissolution of feldspar. As a consequence of feldspar dissolution, a secondary pore space was generated. This included intragranular dissolution pores developed within mineral grains and intergranular dissolution pores developed between mineral grains, with the latter being more predominant. Upon close examination, the rock surface was found to contain a substantial amount of debris and a significant quantity of clay minerals attached to the surface.

4.2. Variation of Fractal Dimension under the Impact of CO_2. Form the nitrogen absorption test results, the package area between the absorption curve and desorption curve had changed, which could reflect the variation of pores volume of shale rock.[33] Although the BET surface area of the Utica Shale sample remained relatively the same after CO_2 exposure, the micropore surface area and volume noticeably decreased and smaller changes were observed in the meso-pore and ultramicro-pore volumes (Sean et al. 2018).[34] The variation of the pore-throat structure could be further analyzed by considering the variation of the fractal dimension of shale rock. The analysis of the fractal dimension of a porous material is related to the characterization of the roughness of the pore surface.[35] One of the methods that appears to be gaining

https://doi.org/10.1021/acsomega.3c09698
ACS Omega 2024, 9, 15259−15270

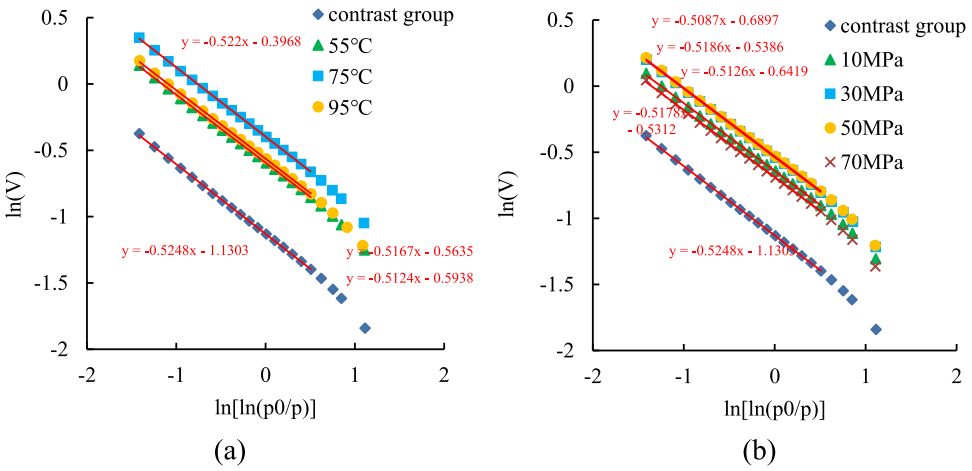

Figure 11. Fitting curves for fractal dimension of different samples (a) fitting curve under different temperature; (b) fitting curve under different pressure.

popularity is the application of the Frenkel−Halsey−Hill theory for the study of the fractal dimensions of shales (eq 5). The surface fractal dimension is calculated by eq 6. It is expressed by a dimensionless number often between two and three, where two is the representation of a perfectly smooth surface (smooth and uniform), and three correspond to rough and disordered surface (complex pore structure, extremely irregular and uneven).[36]

$$\ln(V/V_0) = K\ln[\ln(P_0/P)] + C \tag{5}$$

$$D_s = K + 3 \tag{6}$$

where, V was the adsorption volume of the sample at the equilibrium pressure; V_0 depicted the monolayer coverage volume; P_0 was the saturation vapor pressure of the adsorbed gas; P illustrated the equilibrium pressure of the system; K was a characteristic constant; C was a constant; and D_s was the fractal dimension.

Considering the peak pore size distribution range of the sample in this study, the main focus was on studying the fractal dimension of the high-pressure region. Through analysis of the results of the nitrogen absorption test, the fitting curves for the fractal dimensions of different samples according to eq 5 were obtained as Figure 11. Then the fractal fitting equation and fractal dimension were obtained as Table 3. The median pore size is also shown in Figure 4. The fractal dimension was between 2.4752 and 2.4913, with an average value of 2.4833. The results showed that the fractal dimension values were generally large and the range was narrow, indicating that the pore structure of shale samples in the study was generally complex, moderate rough, and with strong heterogeneity. For the samples with CO_2 treatment under high temperature and pressure conditions, the fractal dimension value increased relative to that without CO_2 treatment. However, there was no obvious change rule or correlation. It indicated that CO_2 increased the complexity of shale samples. The pores in the action area became regular (circular or microcracks expand), but it also led to more pores and greater tortuosity.

Table 3. Values of Fractal Dimension of Different Samples

sample	fractal fitting equation	R^2	fractal dimension	median pore size (nm)
Y-0	$Y = -0.5248X - 1.1303$	0.9998	2.4752	10.52
Y-1	$E = -0.5124X - 0.5938$	0.9998	2.4876	11.58
Y-2	$Y = -0.5220X - 0.3968$	0.9999	2.4780	11.59
Y-3	$Y = -0.5167X - 0.5635$	0.9998	2.4833	10.70
Y-4	$Y = -0.5126X - 0.6419$	0.9997	2.4874	10.73
Y-5	$Y = -0.5186X - 0.5386$	0.9999	2.4814	9.75
Y-6	$Y = -0.5178X - 0.5312$	0.9997	2.4822	11.60
Y-7	$Y = -0.5087X - 0.6897$	0.9997	2.4913	12.65

In addition, the relationship between the porosity from the nitrogen absorption test and mass fractal dimension of the shale samples was studied in Figure 12a. The red point in Figure 12a was that without the CO_2 treatment. CO_2 had an obvious effect on the porosity enhancement. The porosity value was negatively related to the fractal dimension for the samples with CO_2 treatment. The sample with large porosity was usually with smooth pore surface and complex pore-throat network. The relationship between the median pore size and mass fractal dimension of the shale samples was studied in Figure 12b. Similar to the researches,[36] the shale median pore size and mass fractal dimension were shown to have a highly positive correlation, and the correlation coefficient was high. The mass fractal dimension increased with the average pore size. There were also special points that strongly deviated from the fitting line in Figure 12. For the point with a larger value of median pore size and a lower value of fractal dimension (sample Y-2), the shale had a positive effect by CO_2. The porosity was increased and the flow resistance was relatively low. For the point with a lower value of median pore size and a lower value of fractal dimension (sample Y-5), the micropores instead of macropores were mainly influenced, and the surface became smoother. The above relations suggested that there are other factors that influenced the pore-throat structure enhancement effect by CO_2. A complex link was found between the pore-throat structure and fractal dimension. It resulted from the combined relationship between the macropores and micropores in the samples, and the complex function of CO_2.

When the temperature increased and the data of sample Y-2 was neglected, the fractal dimension was found to increase first and decrease then. When the pressure increased, the fractal dimension was found to increase first, decrease then, and increased finally. The variation rule of the fractal dimension resembled the changing rules of specific surface area.

https://doi.org/10.1021/acsomega.3c09698
ACS Omega 2024, 9, 15259−15270

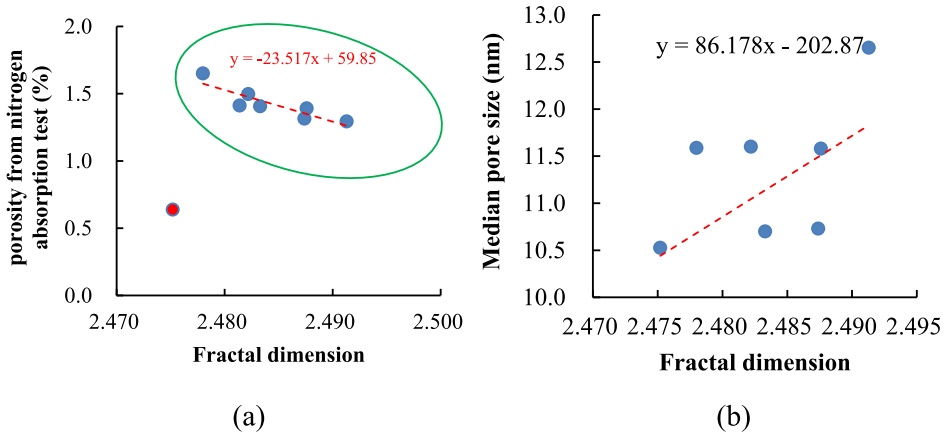

Figure 12. Relationship between the mass fractal dimension and other parameters (a) porosity; (b) median pore size.

When the pressure increased from 10 to 30−70 MPa, CO_2 transitioned from a gaseous state to a supercritical state. Under the condition of 10 MPa, the capillary resistance of CO_2-entering shale was relatively high, and there was a significant Jamin effect. Under high pressure of 30−50 MPa, the ability of supercritical CO_2 to enter mesopores and macropores was significantly enhanced. Therefore, as a result of increasing the contact area with rock pores, the dissolution effect with rock minerals increases, reflecting an increase in the specific surface area after dissolution. Under a high pressure of 70 MPa, supercritical CO_2 should theoretically further enhance the reaction with contact minerals. However, it was thought that the increase in pressure causes CO_2 to further exhibit a multilayer adsorption state, where CO_2 was concentrated in larger pores for reaction, and the CO_2 molecular layer in the contact part reacted with minerals on rock surface in contact. On the other hand, when the CO_2 immersion is completed, the pressure is released, and the CO_2 quickly collided to leave the core pore throat. Along with obvious particle migration, some surface minerals were clearly peeled off and some were piled up near intergranular pores, which might cause bridging or blockage. When further nitrogen adsorption was used to test the pore size, it was impossible to enter these blocked micropores, resulting in a decrease in the actual specific surface area and pore volume tested.

As the temperature increased, the reaction rate between supercritical CO_2 and rock minerals increased and the specific surface area and pore volume of the rock increased after enhanced dissolution. When the temperature was further increased, supercritical CO_2 increased the reaction rate with rock minerals, but the selectivity of the reaction was enhanced, showing enhanced dissolution along the edges of brittle minerals such as feldspar, which affected the dissolution effect on micropore throats. This was manifested as a significant decrease in the relative content of feldspar, illite mixed layer, and chlorite in Figure 2, and an increase in the relative content of clay minerals.

Overall, the changes in micropore size and fractal dimension were analyzed to be the result of comprehensive effects such as mineral dissolution and particle transport after CO_2 release. CO_2 dissolution and particle transport have both positive and negative effects on the effective pores.

Based on the test results of shale porosity, permeability, microscopic pore structure, and mineral composition, the effect of CO_2 on shale dissolution under high temperature and pressure conditions was obvious and the effect of pore dissolution and volume enhancement was outstanding. It provided evidence for supercritical CO_2 injection to increase the physical properties of shale formation so as to increase the shale gas or oil output. However, the effect of CO_2 on permeability might have an increasing trend and a possible weakening trend. Therefore, it is recommended to optimize the temperature and pressure conditions for carbon dioxide action. The action distance should also be considered during the application of supercritical CO_2 in high-pressure and high-temperature situation. The pressure and temperature of CO_2 varied in different distance when CO_2 flow in to the deep layer, inducing the varying phase character of CO_2 and change of physical properties. Extra attention should be put on the experimental results, when a numerical simulation is performed and assuming changing values of porosity and permeability, instead of constant values.

5. CONCLUSIONS

(1) Under high-temperature and high-pressure conditions, supercritical carbon dioxide had an obvious effect on shale minerals and pore structure of shale rock (from Chang 7 layer in Ordos basin). In the experiment on the shale rock, the relative content of plagioclase and potassium feldspar decreased overall, while the relative content of clay minerals fluctuated significantly. There was a minor increase in the relative content of quartz and pyrite. Kaolinite, I/S mixed layer and chlorite displayed a decreasing trend with increasing temperature, while the relative content of illite increased. The dissolution effect of potassium feldspar and plagioclase was evident with microscale observation.

(2) The average BET-specific surface and average total pore volume first increased and then decreased with increasing pressure and temperature of CO_2. The temperature of the CO_2 had a significant effect on the porosity and permeability of the shale. The porosity of shale rock showed an overall increasing trend, but the permeability showed a trend of first increasing and then decreasing. The permeability was mainly enhanced, but a phenomenon of permeability weakness also existed, indicating that the values of high temperature and pressure of supercritical carbon dioxide should be optimized.

https://doi.org/10.1021/acsomega.3c09698
ACS Omega 2024, 9, 15259−15270

AUTHOR INFORMATION

Corresponding Authors

Xiao Sun − *Research Institute of Shaanxi Yanchang Petroleum (Group) Co. Ltd., Xi'an 710065, China; Shaanxi Key Laboratory of Carbon Dioxide Sequestration and Enhanced Oil Recovery, Xi'an 710065, China*; Email: yanchangsunxiao@163.com

Liming Zheng − *School of Vehicle and Energy, Yanshan University, Qinhuangdao 066004, China; Hebei Engineering Research Center for Low Carbon Development and Resource Utilization of Fossil Energy Sources, Yanshan University, Qinhuangdao 066004, China*; orcid.org/0000-0003-1560-1813; Email: upczlm@sina.cn

Authors

Xiangzeng Wang − *Research Institute of Shaanxi Yanchang Petroleum (Group) Co. Ltd., Xi'an 710065, China; Shaanxi Key Laboratory of Carbon Dioxide Sequestration and Enhanced Oil Recovery, Xi'an 710065, China*

Xing Guo − *Research Institute of Shaanxi Yanchang Petroleum (Group) Co. Ltd., Xi'an 710065, China; Shaanxi Key Laboratory of Carbon Dioxide Sequestration and Enhanced Oil Recovery, Xi'an 710065, China; State Key Laboratory of Coal Mine Disaster Dynamics and Control, Chongqing University, Chongqing 400044, China*; orcid.org/0000-0003-2747-4268

Pan Luo − *Research Institute of Shaanxi Yanchang Petroleum (Group) Co. Ltd., Xi'an 710065, China; Shaanxi Key Laboratory of Carbon Dioxide Sequestration and Enhanced Oil Recovery, Xi'an 710065, China*

Complete contact information is available at: https://pubs.acs.org/10.1021/acsomega.3c09698

Notes

The authors declare no competing financial interest.

ACKNOWLEDGMENTS

This work is supported by the National Key Research and Development Program of China under grant (2022YFE0206700), Natural Science Fund of Hebei Province (E2020203013), National Natural Science Foundation of China (52274074) and Natural Science Basic Research Plan in Shaanxi Province of China (2024JC-YBMS-387).

NOMENCLATURE

CO_2, carbon dioxide
$CaCl_2$, calcium chloride
XRD, X-ray diffraction
I/S, mixed layer illite−smectite

REFERENCES

(1) Pamukcu, Y. Z.; Gumrah, F. Simulating oil recovery during CO_2 sequestration into a mature oil reservoir. In *Paper presented at the Canadian International Petroleum Conference, PETSOC-2007-017*, Calgary, Alberta, 2007.

(2) Iogna, A.; Guillet-Lhermite, J.; Wood, C.; Deflandre, J. P. CO_2 storage and enhanced gas recovery: using extended black oil modelling to simulate CO_2 injection on a North Sea depleted gas field. In *Paper presented at the SPE Europec featured at 79th EAGE Conference and Exhibition, SPE-185859-MS*, Paris, France, 2017.

(3) Abu Bakar, M. A.; Wan Mohamad, W. A.; Moh Wahi, M. W.; Amir, S. Material selection and corrosion rate analysis for CO_2 injection well: a case study of K1 field CO_2 sequestration project. In *Paper presented at the International Petroleum Technology Conference, Virtual, IPTC-21818-MS*, 2021.

(4) Lang, D.; Lun, Z.; Lyu, C.; Wang, H.; Zhao, Q.; Sheng, H. Nuclear magnetic resonance experimental study of CO_2 injection to enhance shale oil recovery. *Pet. Explor. Dev.* **2021**, *48* (3), 702−712.

(5) Sui, H.; Zhang, F.; Zhang, L.; Wang, Z.; Yuan, S.; Wang, D.; Wang, Y. Mechanism of CO_2 enhanced oil recovery in kerogen pores and CO_2 sequestration in shale: A molecular dynamics simulation study. *Fuel* **2023**, *349*, 128692.

(6) Wei, J.; Li, J.; Zhou, X.; Zhang, X. Effect of pressure and CO_2 content on the asphaltene precipitation in the light crude oil. *Pet. Sci. Technol.* **2020**, *38* (2), 116−123.

(7) Li, L.; Su, Y.; Lv, Y.; Tu, J. Asphaltene deposition and permeability impairment in shale reservoirs during CO_2 huff-n-puff EOR process. *Pet. Sci. Technol.* **2020**, *38* (4), 384−390.

(8) Yang, K.; Zhou, J.; Xian, X.; Zhang, C.; Gan, Q.; Dong, Z. Effect of supercritical CO_2-water-shale interaction on mechanical properties of shale and its implication for carbon sequestration. *Gas Sci. Eng.* **2023**, *111*, 204930.

(9) Chao, Z.; Zhaomin, L.; Dong, Z. Experimental research on the influence of supercritical CO_2 flooding on reservoir physical property. *J. Southwest Pet. Univ.* **2013**, *35* (5), 94−98.

(10) Li, N.; Jin, Z.; Wang, H.; Zou, Y.; Zhang, S.; Li, F.; Zhou, T.; Jiang, M. Investigation into shale softening induced by water/CO_2-rock interaction. *Int. J. Rock Mech. Min. Sci.* **2023**, *161*, 105299.

(11) Tian, S.; Zhou, J.; Xian, X.; Gan, Q.; Yang, K.; Zheng, Y.; Deng, G.; Zhang, F. Impact of supercritical CO_2 exposure time on the porosity and permeability of dry and wet shale: The influence of chemo-mechanical coupling effects. *Energy* **2023**, *270*, 126905.

(12) Jafari Behbahani, T.; Ghotbi, C.; Taghikhani, V.; Shahrabadi, A. Experimental study and mathematical modeling of asphaltene deposition mechanism in core samples. *Oil Gas Sci. Technol. - Rev. d'IFP Energies Nouvelles* **2015**, *70* (6), 1051−1074.

(13) Shen, Z.; Sheng, J. J. Investigation of asphaltene deposition mechanisms during CO_2 huff-n-puff injection in Eagle Ford shale. *Pet. Sci. Technol.* **2017**, *35* (20), 1960−1966.

(14) Yong, T.; Wenjun, H.; Yiyang, J.; Liying, F.; Xiang, S.; Yi, Z.; Menglin, Z.; Jian, C.; et al. Enrichment conditions and exploration direction of Permian saline lacustrine shale oil and gas in Junggar Basin. *Acta Petrolei Sin.* **2023**, *44* (1), 125−143.

(15) Ji, C.; Xiaofeng, Y.; Teng, M. Petroleum exploration in China: 2022 review and 2023 outlook. *Nat. Gas Technol. Econ.* **2023**, *17* (2), 1−10.

(16) Wei, L.; Hua, Z.; Yongliang, H.; et al. Prepad supercritical carbon dioxide fracturing technology in shale oil reservoir. *Well Test.* **2023**, *32* (1), 38−44.

(17) Xie, W.; Wang, M.; Wang, H. Adsorption Characteristics of CH4 and CO_2 in Shale at High Pressure and Temperature. *ACS Omega* **2021**, *6*, 18527−18536.

(18) Xie, W.; Wang, H.; Vandeginste, V.; Chen, S.; Gan, H.; Wang, M.; Yu, Z. Thermodynamic and kinetic affinity of CO_2 relative to CH_4 and their pressure, temperature and pore structure sensitivity in the competitive adsorption system in shale gas reservoirs. *Energy* **2023**, *277*, 127591.

(19) Jie, L.; Lei, Z. Effects of supercritical CO_2 at different temperatures on shale mechanical properties. *Min. Res. Dev.* **2021**, *41* (5), 80−81.

(20) Lianchao, J.; Pengfei, L.; Dan, Y.; et al. Experiment of enhancing the recovery of the shale adsorbed gas by CO_2 injection: taking Yanchang-formation Chang-7 shale gas in Ordos Basin as an example. *Pet. Geol. Oilfield Dev. Daqing* **2021**, *40* (2), 153−159.

(21) Fengjun, Z.; Huaiyuan, W.; Guanghua, W.; et al. Experiment on mechanism of CO_2CO_2 fluid interacting with sandstone layer. *J. Jilin Univ.* **2012**, *42* (3), 821−826.

(22) Thommes, M.; Kaneko, K.; Neimark, A. V.; Olivier, J. P.; Rodriguez-Reinoso, F.; Rouquerol, J.; Sing, K. S. W. Physisorption of gases, with special reference to the evaluation of surface area and pore size distribution (IUPAC Technical Report). *Pure Appl. Chem.* **2015**, *87*, 1052−1069.

(23) Qin, C.; Jiang, Y.; Zuo, S.; Chen, S.; Xiao, S.; Liu, Z. Investigation of adsorption kinetics of CH4 and CO_2 on shale exposure to supercritical CO_2. *Energy* **2021**, *236*, 121410.
(24) Xiaoming, L.; Yarong, W.; Wen, L.; Ma, L.; Liu, D.; Liu, J.; Zhang, Y. Micro-pore structure and fractal characteristics of deep shale from Wufeng Formation to Longmaxi Formation in Jingmen exploration area, Hubei Province, China. *J. Nat. Gas Geosci.* **2022**, *7* (3), 121−132.
(25) Yanxia, P.; Yushan, D.; Long, J.; et al. Micropore structure and fractal characteristics of shale oil reservoir in gentle slope zone of Jiyang Depression. *Fault-Block Oil Gas Field* **2023**, *30* (4), 535−544.
(26) Zhan, H.; Li, X.; Hu, Z.; Duan, X.; Wu, W.; Guo, W.; Lin, W. Fractal Characteristics of Deep Shales in Southern China by Small-Angle Neutron Scattering and Low-Pressure Nitrogen Adsorption. *Fractal Fract.* **2022**, *6*, 484.
(27) Yin, H.; Zhou, J.; Jiang, Y.; Xian, X.; Liu, Q. Physical and structural changes in shale associated with supercritical CO_2 exposure. *Fuel* **2016**, *184*, 289−303.
(28) Fatah, A.; Mahmud, H. B.; Bennour, Z.; Hossain, M.; Gholami, R. Effect of supercritical CO_2 treatment on physical properties and functional groups of shales. *Fuel* **2021**, *303*, 121310.
(29) Kaile, Y.; Shenglin, H.; Zhaoqiang, Y.; et al. Diagenesis characteristics of tight sandstone reservoirs with high temperature, overpressure and high CO_2CO_2 content: A case study of Neogene Meishan-Huangliu Formation in LD10 area, Yinggehai Basin. *Lithologic Reservoirs* **2023**, *35* (1), 83−95.
(30) Xinjing, P.; Mengqi, L.; Xiangbin, X.; et al. Interaction of rock-brine-supercritical CO_2CO_2 in sandstone reservoir. *J. China Univ. Min. Technol.* **2013**, *42* (2), 302−307.
(31) Zou, Y.; Li, S.; Ma, X.; Zhang, S.; Li, N.; Chen, M. Effects of CO_2−brine−rock interaction on porosity/permeability and mechanical properties during supercritical-CO_2 fracturing in shale reservoirs. *J. Nat. Gas Sci. Eng.* **2018**, *49*, 157−168.
(32) Shugang, Y.; Mingyu, C.; Kunfeng, Z.; et al. Research progress and prospect of CO_2CO_2-water-rock interaction on petrophysical properties of CO_2CO_2 geological sequestration. *Pet. Geol. Recovery Effic.* **2023**, *30* (6), 80−91.
(33) Zhu, H.; Gao, J.; Yang, M.; Shi, E.; Lu, Y.; Qi, Y.; Wei, M.; Wang, W. A Comparative Study on the Microstructure and Petrophysical Properties of Undeformed and Naturally Deformed Shales. *Energy Fuels* **2023**, *37*, 1917−1928.
(34) Sanguinito, S.; Goodman, A.; Tkach, M.; Kutchko, B.; Culp, J.; Natesakhawat, S.; Fazio, J.; Fukai, I.; Crandall, D. Quantifying dry supercritical CO_2-induced changes of the Utica Shale. *Fuel* **2018**, *226*, 54−64.
(35) Hui, D.; Pan, Y.; Luo, P.; Zhang, Y.; Sun, L.; Lin, C. Effect of supercritical CO_2 exposure on the high-pressure CO_2 adsorption performance of shales. *Fuel* **2019**, *247*, 57−66.
(36) Medina-Rodriguez, B. X.; Alvarado, V. Use of Gas Adsorption and Inversion Methods for Shale Pore Structure Characterization. *Energies* **2021**, *14*, 2880.

https://doi.org/10.1021/acsomega.3c09698
ACS Omega 2024, 9, 15259−15270